

Experimental and Theoretical Studies on Carbon–Nitrogen Clusters $C_{2n}N_7^-$

Shutao Sun, Yali Cao, and Zhang Sun

State Key Laboratory of Molecular Reaction Dynamics, Center of Molecular Science, Institute of Chemistry, Chinese Academy of Sciences, Beijing 100080, P. R. China

Zichao Tang*

State Key Laboratory of Molecular Reaction Dynamics, Dalian Institute of Chemical Physics, Chinese Academy of Sciences, Dalian 116023, P. R. China

Lansun Zheng

State Key Laboratory for Physical Chemistry of Solid Surfaces, Department of Chemistry, Xiamen University, Xiamen, Fujian 361005, P. R. China

Received: December 30, 2005; In Final Form: March 31, 2006

$C_{2n}N_7^-$ cluster ions are produced by laser ablating on the $K_3[Fe(CN)_6]$ sample. DFT calculations have been performed for these cluster anions. Various isomeric structures of these clusters are optimized and their energies are compared to find the most stable isomers. The most stable structure for $C_8N_7^-$ is similar to that of adenine by theoretical calculation, which is in agreement with the collision-induced dissociation (CID) experimental results. With the increasing even numbers of C atoms from 8 to 16, the N atoms in the double-ring structure are gradually substituted by C atoms from the six-membered ring to the five-membered ring. All these $C_{2n}N_7^-$ ($n = 3-9$) clusters exhibit planar aromatic characters. The energy difference and incremental binding energy analyses show that $C_{2n}N_7^-$ ($n = 4-8$) clusters are more stable than $C_6N_7^-$ and $C_{18}N_7^-$, which are consistent with the observed mass spectrum.

1. Introduction

Carbon clusters containing nitrogen atoms have attracted increasing interest in recent years in both fundamental research and application study. In addition, carbon–nitrogen clusters have evoked great interest in interstellar space research since the discovery of such species there in the 70's.¹⁻⁶

Extensive efforts have been made on the experimental investigations on nitrogen-doped carbon clusters. Carbon–nitrogen clusters have been produced by various means, such as laser ablation,⁷⁻⁹ arc discharge,¹⁰⁻¹² vapor deposition,^{13,14} organic synthesis,¹⁵⁻¹⁸ and some other methods.¹⁹⁻²¹ The stable clusters may be used as the building block for cluster-assemble materials, as well as some clusters with new properties having the potential for application. Especially, attention on crystalline β - C_3N_4 , which is expected to possess diamond-like mechanical, optical, and electrical properties, has been increased exponentially in recent years.²²⁻³⁰

Many theoretical studies have also been reported on the carbon–nitrogen clusters. It has been shown that small carbon–nitrogen clusters of $C_nN/C_nN^+/C_nN^-$ and $C_nN_2/C_nN_2^+/C_nN_2^-$ are linear with the nitrogen atom located on the end of the carbon chain.³¹⁻³⁷ Very recently, Chen et al. carried out DFT calculation on $C_nN_3^-$ ($n = 1-8$) and found that the three branched structures with a nitrogen atom located at each end are the ground states for $n = 3-8$.³⁸ All the above carbon–nitrogen clusters containing one to three nitrogen atoms show odd/even alternation in stabilities. As to the carbon–nitrogen clusters containing more nitrogen atoms, Tang et al. studied

the structures of $C_{2n}N_5^-$ combined the CID experiment and DFT calculation, revealing that the cyano-substituted, planar five-membered ring structures are most stable.³⁹ To the best of our knowledge, there is no report of the systematic studies on the structures of carbon–nitrogen clusters containing more than five nitrogen atoms.

Interestingly, our group has obtained the stable mass peaks of $C_{2n}N_7^-$ by tandem time-of-flight mass spectrometer (TOF-MS) through laser ablation on the $K_3[Fe(CN)_6]$ sample and also probed their structures by the collision-induced dissociation experiment.⁷ Recently, we made progress in the structure research of these clusters combining experimental and theoretical investigations. We find that the lowest energy structures for $C_{2n}N_7^-$ ($n = 3-9$) are planar double-ring structures, with $-CN$ groups being the substituents. All these $C_{2n}N_7^-$ products present aromatic characteristics.

2. Experimental Methods

The $C_{2n}N_7^-$ cluster ions were produced by laser ablation on $K_3[Fe(CN)_6]$ sample. The pulsed laser beam was the second harmonic of a Nd:YAG laser (10 Hz, 532 nm wavelength, 7 ns pulse width), and focused with a lens to approximately a 1 mm spot on the sample with a power intensity of the order of 10^8 W cm^{-2} . The sample was located 6 cm away from the exit of the acceleration electrodes. The cluster ions were formed in the laser vaporized plasma and entered the acceleration region of the mass spectrometer by their initial kinetic energy.

The voltage to the first pulsed acceleration field of the mass spectrometer was applied at 950 eV. After passage through a 250 cm field-free drift tube, cluster ions with different masses

* Address correspondence to this author. E-mail: zctang@iccas.ac.cn.

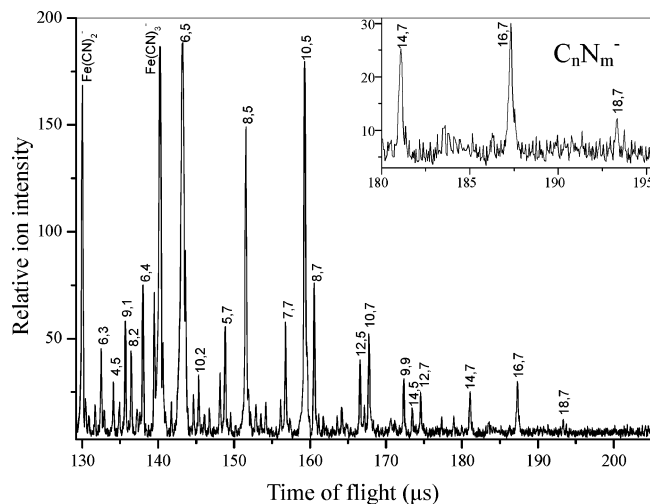


Figure 1. Time-of-flight mass spectrum of $C_n N_m^-$ cluster ions produced by laser ablation on the $K_3[Fe(CN)_6]$ sample. The mass peak of each $C_n N_m^-$ cluster ion is labeled by (n,m) , in which n is the number of carbon atoms and m is the number of nitrogen atoms.

were separated and recorded. Mass resolution for the first stage of the tandem mass spectrometer exceeds 400. The mass gate located at the end of the first drift tube has a pulsed electric field, and can select a cluster ion with a specified mass. The selected cluster ions were then decelerated and crossed with a supersonic molecular beam. After collisions, both the parent and daughter ions were reaccelerated and mass analyzed according to their different flight times through a second field-free drift tube. The acceleration voltage applied in the second stage was 3000 V, and mass resolution in this stage was near 100. The output ion signal from the dual-microchannel-plate detector was digitized by a 100 megasample s^{-1} transient digitizer after preamplification.

The $K_3[Fe(CN)_6]$ sample (purity >99%) was pressed into the sample holder before the experiment. The supersonic molecular beam was controlled by a pulsed valve. Under normal operating conditions, the background pressure of the collision chamber was approximately 3×10^{-5} Torr. The back pressure of the valve was $(2-4) \times 10^5$ Pa. For the experiment, nitrogen of high purity was used as a buffer gas to collide with the cluster ions.

3. Computational Methods

Various initial geometric structures were selected for initial optimization in this work. For the constituent groups, we have considered different functional groups, e.g., cyano ($-CN$), isocyano ($-NC$), $-C_3N$, and $-C_5N$. According to the optimization results on the different initial geometries for the $C_6N_5^-$ cluster (Figure 1S and Table 1S, Supporting Information), we can see that the most stable termination group is the cyano group ($-CN$). So we take the cyano group substituted isomers as the primary geometries to calculate for the products in this work. Initial geometry optimizations were performed at the B3LYP/6-31G(d) level and we found that the double-ring isomers are reasonable. Then the larger basis sets, 6-31+G(d) and 6-311G(d), are also employed to perform the optimizations and frequencies analysis. These anionic structures were finally reoptimized at the B3LYP/6-311+G(d) level. Harmonic vibrational frequencies were calculated again at the final level to characterize the stationary point as the minimum. The calculation results with the above basis sets are consistent. The data of partial charges were analyzed with natural bond orbital (NBO). All the calculations were carried out using the Gaussian 98 program.⁴⁰

TABLE 1: Composition and Relative Abundance of Daughter Ions Dissociated from $C_6N_5^-$ and $C_{2n}N_7^-$ ($n = 4, 7, 8$)

parent ions	daughter ions (relative % abundance)				
$C_6N_5^-$	CN^- (60)	$C_4N_3^-$ (40)			
$C_8N_7^-$	CN^- (40)	$C_3N_2^-$ (10)	$C_4N_3^-$ (25)	$C_6N_5^-$ (25)	
$C_{14}N_7^-$	CN^- (10)	$C_4N_3^-$ (18)	$C_6N_5^-$ (41)	$C_6N_5^-$ (31)	
$C_{16}N_7^-$	CN^- (9)	$C_6N_5^-$ (42)	$C_6N_5^-$ (26)	$C_8N_5^-$ (23)	

TABLE 2: Symmetries, Electronic States, Total Energies, Relative Energies, and Lowest Vibrational Frequency for $C_{2n}N_7^-$ ($n = 3-9$) Isomers at the B3LYP/6-311+G(d) Level

	isomer	sym	state	E_{total}^a (hartree)	ΔE (eV)	lowest vib freq (cm^{-1})	
$C_6N_7^-$	A	C_s	$^1A'$	-612.015819	0.0000	70.7	
	B	C_s	$^1A'$	-612.002145	0.3721	102.6	
	C	C_{2v}	1A_1	-611.995899	0.5420	84.9	
	D	C_s	$^1A'$	-611.981530	0.9330	68.7	
	E	C_s	$^1A'$	-611.957329	1.5915	66.5	
	F	C_s	$^1A'$	-611.957233	1.5941	65.5	
	G	C_{2v}	1A_1	-611.953146	1.7053	102.5	
$C_8N_7^-$	A	C_s	$^1A'$	-688.265169	0.0000	70.4	
	B	C_{2v}	1A_1	-688.260549	0.1257	67.2	
	C	C_{2v}	1A_1	-688.231734	0.9098	74.4	
	D	C_s	$^1A'$	-688.217573	1.2951	60.0	
	E	C_{2v}	1A_1	-688.173854	2.4847	71.5	
	$C_{10}N_7^-$	A	C_s	$^1A'$	-764.478726	0.0000	53.7
		B	C_s	$^1A'$	-764.477069	0.0451	60.4
C		C_s	$^1A'$	-764.474759	0.1079	50.3	
D		C_s	$^1A'$	-764.474682	0.1100	53.1	
E		C_{2v}	1A_1	-764.462633	0.4379	48.8	
F		C_s	$^1A'$	-764.440949	1.0279	53.6	
G		C_{2v}	1A_1	-764.433013	1.2439	45.5	
H		C_{2v}	1A_1	-764.431735	1.2786	62.0	
I		C_s	$^1A'$	-764.428990	1.3533	44.2	
J		C_s	$^1A'$	-764.428984	1.3535	42.0	
K		C_s	$^1A'$	-764.428350	1.3707	44.6	
$C_{12}N_7^-$	A	C_{2v}	1A_1	-840.692389	0.0000	53.1	
	B	C_s	$^1A'$	-840.686516	0.1598	48.8	
	C	C_s	$^1A'$	-840.686305	0.1655	51.1	
	D	C_s	$^1A'$	-840.685868	0.1774	54.5	
	E	C_s	$^1A'$	-840.685136	0.1974	50.9	
	F	C_{2v}	1A_1	-840.682313	0.2742	49.2	
	G	C_s	$^1A'$	-840.677577	0.4030	44.7	
	H	C_s	$^1A'$	-840.677351	0.4092	45.8	
	I	C_{2v}	1A_1	-840.650292	1.1455	44.1	
	J	C_s	$^1A'$	-840.643401	1.3330	37.2	
	K	C_s	$^1A'$	-840.642483	1.3579	34.6	
	L	C_s	$^1A'$	-840.642459	1.3586	42.6	
	M	C_s	$^1A'$	-840.642269	1.3638	39.4	
$C_{14}N_7^-$	A	C_s	$^1A'$	-916.898853	0.0000	50.2	
	B	C_s	$^1A'$	-916.895365	0.0949	44.7	
	C	C_s	$^1A'$	-916.894415	0.1208	42.7	
	D	C_{2v}	1A_1	-916.889364	0.2582	43.2	
	E	C_{2v}	1A_1	-916.856159	1.1617	36.4	
$C_{16}N_7^-$	A	C_{2v}	1A_1	-993.105452	0.0000	41.2	
	B	C_s	$^1A'$	-992.923284	4.9568	22.4	
	C	C_s	$^1A'$	-992.923158	4.9602	20.3	
$C_{18}N_7^-$	A	C_s	$^1A'$	-1069.271042	0.0000	28.6	
	B	C_s	$^1A'$	-1069.270621	0.0115	29.0	
	C	C_{2v}	1A_1	-1069.270299	0.0202	32.8	
	D	C_s	$^1A'$	-1069.270023	0.0277	30.2	

^a E_{total} includes a correction for zero-point vibrational energies.

4. Results

4.1. TOF-MS Results. Figure 1 shows the mass spectrum of the cluster anions resulting from laser ablation on the $K_3[Fe(CN)_6]$ sample. A series of binary carbon–nitrogen cluster anions are formed, and $C_{2n}N_7^-$ anions are the products with the largest mass in the spectrum. The $C_{2n}N_7^-$ clusters appear from $C_8N_7^-$ with the smallest size and strongest signal intensity. When the even number of carbons increases from 8 to 12, the

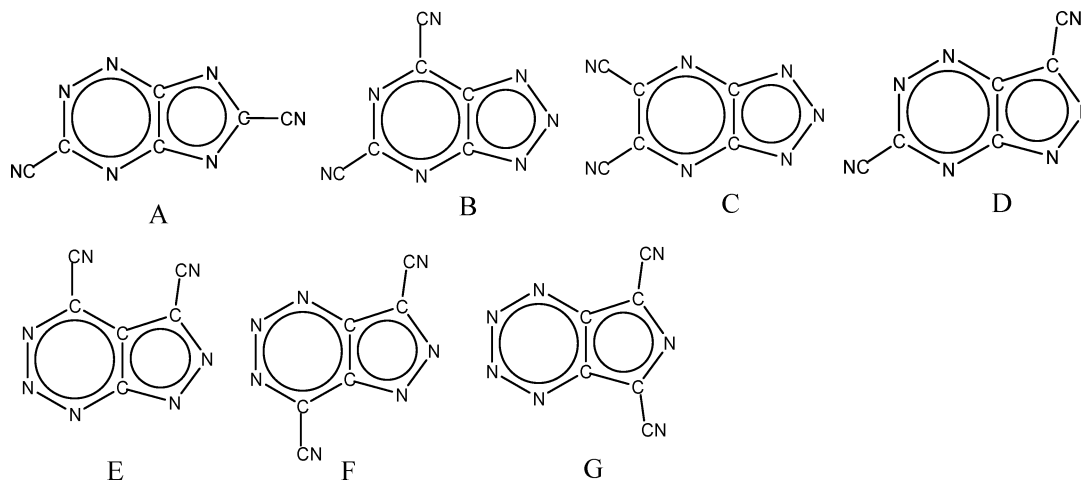


Figure 2. Optimized isomers for $C_6N_7^-$. See Table 2 for their energetic parameters. Groups $-CN$, $-C_3N$, and $-C_5N$ in this and subsequent figures are equal to $-C\equiv N$, $-C\equiv C-C\equiv N$, and $-C\equiv C-C\equiv C-C\equiv N$, respectively.

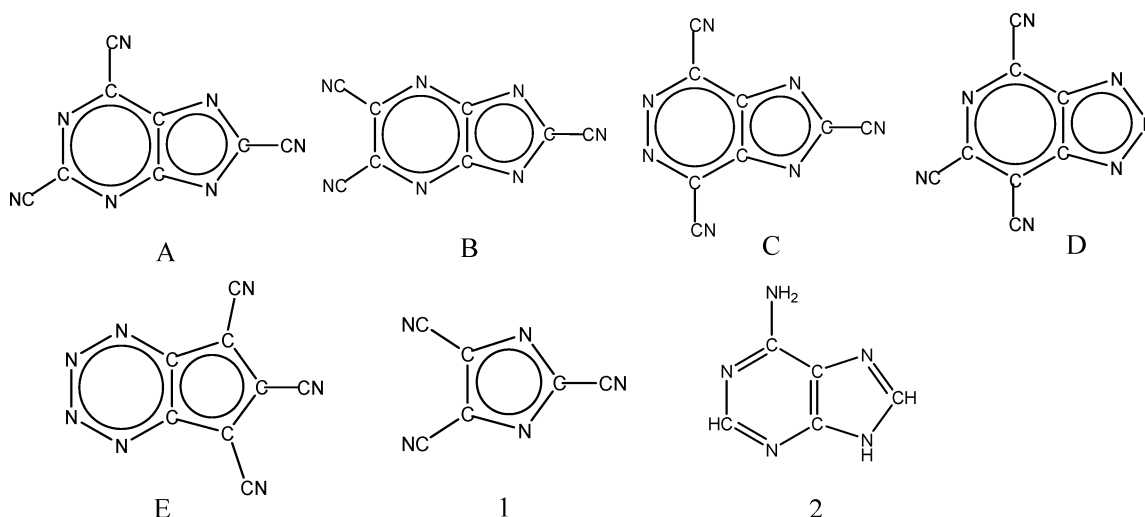


Figure 3. Optimized isomers for $C_8N_7^-$ (A–E), and structures for $C_6N_5^-$ (1) and adenine (2).

cluster intensity decreases in succession, but then increases from $C_{14}N_7^-$ to $C_{16}N_7^-$ and drops suddenly leading to a very weak signal for $C_{18}N_7^-$, and then nearly no signals in the larger mass area. We have also used $K_4[Fe(CN)_6]$ and $C_2(CN)_4$ as the precursors to repeat this experiment under the same conditions, but only the binary cluster ions with one nitrogen atom can be observed from the $K_4[Fe(CN)_6]$ sample and some compounds with multi-nitrogen atoms ($C_nN_m^-$, $n \leq 5$) were obtained from the $C_2(CN)_4$ sample, both without $C_{2n}N_7^-$ species present from these two precursors.

4.2. CID Results. The CID experimental results may shed light on the structures for the clusters by combining the calculation results.^{41,42} Therefore, the CID experiments were performed on the $C_{2n}N_7^-$ ($n = 4, 7, 8$) species. The parent ions and their daughter ions, as well as the relative abundance (presented as a percent of the total ion yield) for the daughter ions, are listed in Table 1. Multistep collisions and fragmentation were observed under the experimental conditions.

4.3. Structures. Shown in Figures 2–8 are the isomers corresponding to local minima of $C_{2n}N_7^-$ ($n = 3–9$) with real vibrational frequencies. In each figure, the isomers are arranged in the order of ascending total energy. The corresponding symmetries, electronic states, total energies, relative energies and lowest vibrational frequencies for these isomers are summarized in Table 2.

5. Discussions

5.1. Geometries and Stabilities. *5.1.1. $C_6N_7^-$.* Though there is no obvious mass peak for $C_6N_7^-$ present in the mass spectrum, we have also investigated the structures for this cluster based on density functional calculations. The lowest energy isomer for this cluster is a double-ring structure with a N–N bond (1.329 Å, between the single bond length of N–N 1.45 Å and the double bond length of N=N 1.23 Å) in the six-membered ring part as shown in Figure 2A. The other isomers with the two $-CN$ groups in other positions have relatively high energy.

5.1.2. $C_8N_7^-$. The CID experiment is performed for the $C_8N_7^-$ cluster and the daughter ions in this experiment are CN^- , $C_3N_2^-$, $C_4N_3^-$, and $C_6N_5^-$ as shown in Table 1. To analyze the structure of $C_8N_7^-$ with the CID result, we first discuss another abundant cluster besides the $C_{2n}N_7^-$ series products— $C_6N_5^-$, which has been studied in our previous work and is a planar aromatic five-membered ring structure.³⁹ The aromatic character of $C_6N_5^-$ is shown by the MOs (molecular orbitals) in Figure 9. Five p- π electrons in the three C atoms and two N atoms in the molecular ring plus one additional electron of the anion cluster make this molecular ring satisfy the $(4n+2)$ Hückel rule and exhibit aromaticity. In the CID experiment, $C_6N_5^-$ is found to be very stable to dissociate, and only two daughter ions CN^- and $C_4N_3^-$ are observed even when the collision energy of parent ions with the crossed supersonic molecular beam is raised to above 150

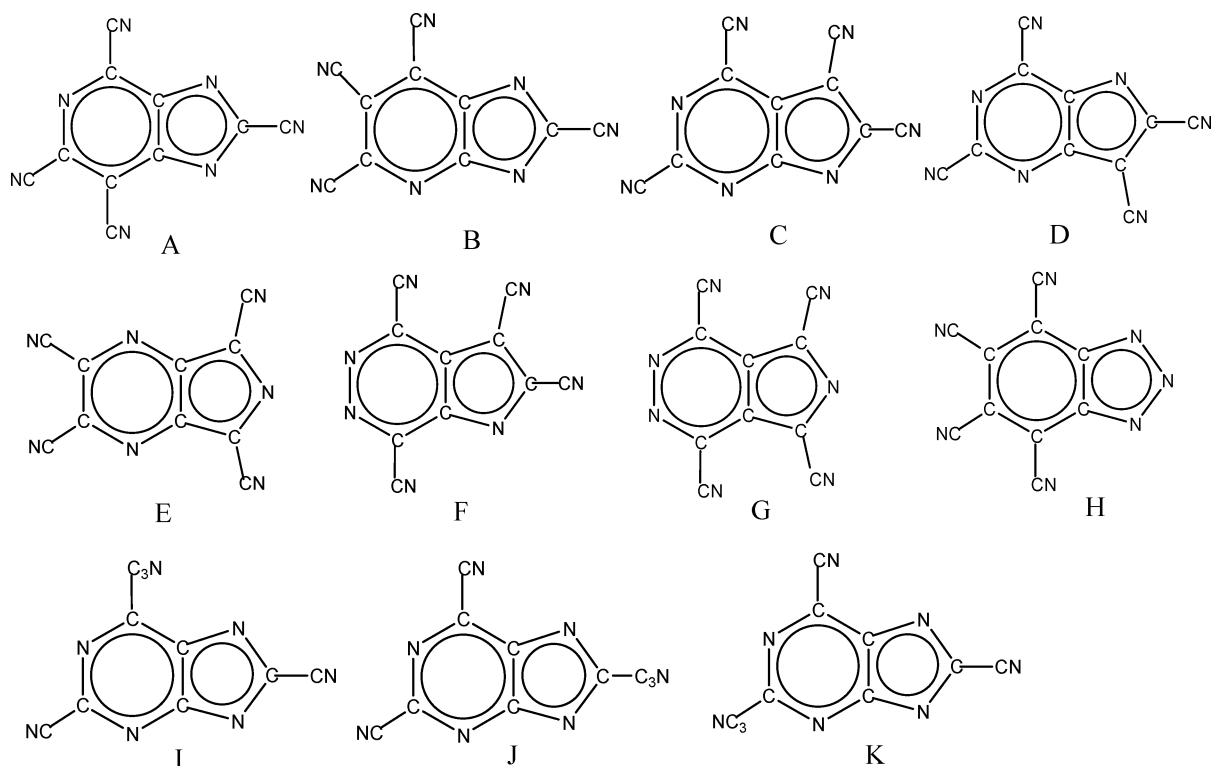
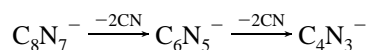


Figure 4. Optimized isomers for $C_{10}N_7^-$.

eV. In the CID experiment of $C_8N_7^-$, abundant CN^- , $C_6N_5^-$, $C_4N_3^-$, and $C_3N_2^-$ fragments are observed, and the $C_4N_3^-$ and CN^- are the right daughter ions of $C_6N_5^-$. On the basis of an analysis of these experimental results, we conclude that $C_8N_7^-$ has a similar structure with $C_6N_5^-$, forming another six-membered heterocyclic ring besides the five-membered ring. With the CID experimental results, the primary dissociation process of $C_8N_7^-$ can be shown as:



What is more interesting, with the calculation results at the B3LYP/6-311+G(d) level, the lowest energy isomer for $C_8N_7^-$ is a double-ring structure similar to that of adenine, with the three substituents being $-CN$ groups. Adenine is the basic component of DNA and RNA. There is a molecular structure of adenine from the XRD (X-ray diffraction) experiment to indicate that adenine is in an aromatic bicyclic configuration.⁴³ As the target products in this work are anion species, we calculated the deprotonation of the adenine anion structure, whose molecular double-ring backbone is the same as that of $C_8N_7^-$. According to the comparison, there is no obvious change for the skeleton double-ring after $-NH_2$ and $-H$ in adenine are substituted by the three $-CN$ groups in $C_8N_7^-$. The difference for the bond length is smaller than 0.02 Å and that for the bond angle is smaller than 1°, but the $-NH_2$ group deviates slightly from the ring plane, while the $C_8N_7^-$ containing three $-CN$ are in a planar coordinate. Because the electronegativity of N is larger than that of C, N atoms carry negative charges, while C atoms are positive in $C_8N_7^-$. As to the whole molecule, natural charge analyses display that the negative charge is mainly distributed on the double-ring ($-0.88|e|$) rather than on the $-CN$ groups. From the delocalized MOs (Figure 9), we can see that it is also a consecutive conjugated aromatic species that resulted from the presence of one negative charge

and nine p- π electrons from the five C atoms and four N atoms in the bicyclic backbone. The other isomers, even with a high geometric symmetry (C_{2v} , Figure 3B,C,E), have higher energy than the adenine-like structure (C_s , Figure 3A).

5.1.3. $C_{10}N_7^-$, $C_{12}N_7^-$, and $C_{14}N_7^-$. The CID experiments are carried out on the $C_{14}N_7^-$ cluster, not on $C_{10}N_7^-$ and $C_{12}N_7^-$ due to their adjacencies with the neighboring mass peaks. The daughter ions of $C_{14}N_7^-$ in the CID experiment include CN^- , $C_4N_3^-$, $C_6N_3^-$, and $C_6N_5^-$ fragments (Table 1). The $C_6N_3^-$ daughter ion is abundant, which indicates that the $C_6N_3^-$ fragment is existent in this cluster structure. For the other three daughter ions CN^- , $C_4N_3^-$, and $C_6N_5^-$, as in the cases in the CID results of $C_6N_5^-$ and $C_8N_7^-$ species, CN^- and $C_4N_3^-$ are also the daughter ions of $C_6N_5^-$, which indicates that there are some similarities in structures of these products.

DFT calculations are performed to find the most stable isomers for these products. With increasing even number of the carbon atoms in these clusters, the N atoms in the ring are gradually substituted by a C atom and a $-CN$ group. The N atom in the ring of $C_8N_7^-$, which has relatively less negative charge (NBO charge: $-0.42|e|$) compared with other N atoms in the double-ring, is substituted by a C atom and a $-CN$ group, forming the $C_{10}N_7^-$ cluster. And the other atoms and configuration remain unchangeable. This lowest energy isomer of $C_{10}N_7^-$ has the $C_6N_3^-$ fragment, which is in agreement with the CID results. The other isomers (I, J, and K in Figure 4), which have the same double-ring frame with $C_8N_7^-$ and only the substituent group $-CN$ is stretched to $-C_3N$, have higher energy. Likewise, $C_{10}N_7^-$ to $C_{12}N_7^-$, the carbon chain extended isomers for the $-CN$ group in the most stable structure of $C_{10}N_7^-$ to form the isomers of $C_{12}N_7^-$, have relatively high energy (J, K, L, and M in Figure 5). The N atom with relatively less negative charge ($-0.42|e|$) in the ring of $C_{10}N_7^-$ being substituted by the C atom and a $-CN$ group gives the most stable structure (Figure 5A) for $C_{12}N_7^-$. $C_{12}N_7^-$ is a C_{2v} symmetry structure with the six-membered ring composed of

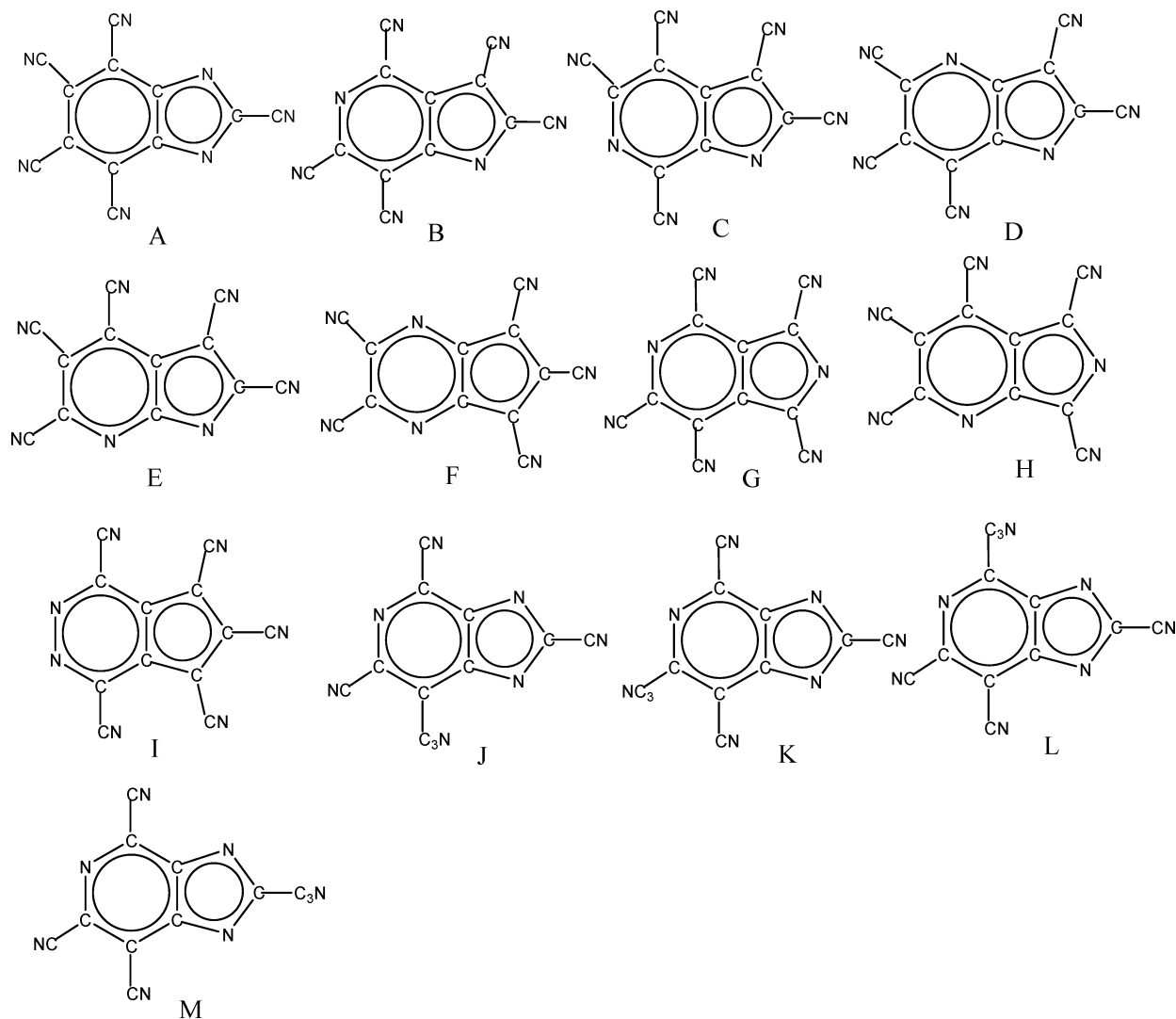


Figure 5. Optimized isomers for $C_{12}N_7^-$.

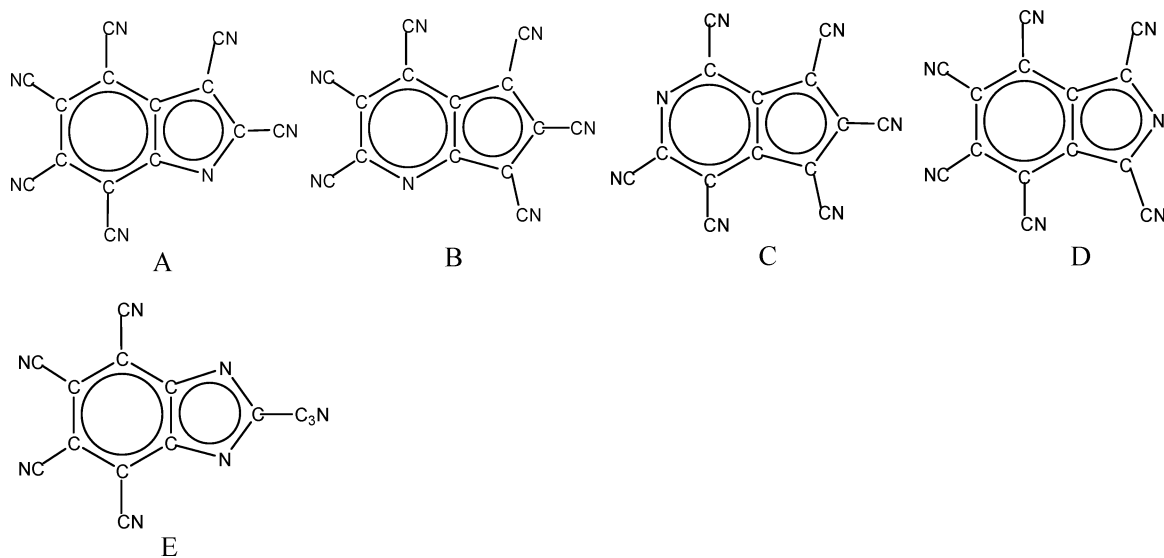


Figure 6. Optimized isomers for $C_{14}N_7^-$.

all C atoms. When the cluster size grows to $C_{14}N_7^-$, the N atom in the five-membered ring begins being substituted by the C atom and a $-CN$ group linked to it. Like the $C_8N_7^-$ cluster, the heterocyclic anions $C_{10}N_7^-$, $C_{12}N_7^-$, and $C_{14}N_7^-$ all have aromatic characteristics. The delocalized π orbitals are formed

from the sp^2 hybridization of C atoms and sp^2 hybridization of N atoms in the double-ring.

5.1.4. $C_{16}N_7^-$. The daughter ions of $C_{16}N_7^-$ in the CID experiment are CN^- , $C_6N_3^-$, $C_6N_5^-$, and $C_8N_5^-$. The $C_6N_3^-$ fragment is most abundant in the ion percent and $C_8N_5^-$ is the

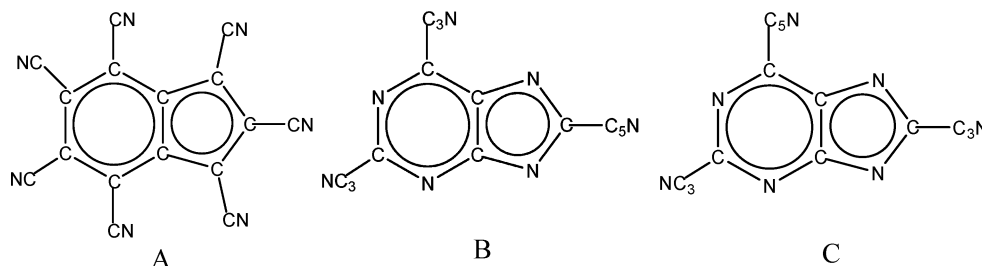


Figure 7. Optimized isomers for $C_{16}N_7^-$.

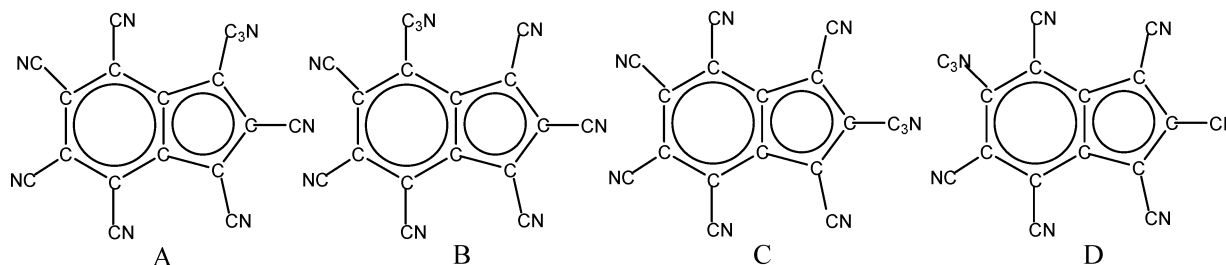


Figure 8. Optimized isomers for $C_{18}N_7^-$.

fragment ion that is not obtained from the CID of the mother ion $C_{14}N_7^-$. On the basis of the DFT calculation result, $C_{16}N_7^-$ is a C_{2v} symmetry structure with the double-ring frame composed of all C atoms, and seven $-CN$ groups are coordinated to the seven-ringed C atoms. So its electron density in the double-ring is more uniform than those of the other heterocyclic products in the $C_{2n}N_7^-$ series. The HOMO to HOMO-3 and HOMO-7 (Figure 9) reveal delocalized binding interaction between the C atoms in the rings and binding between the constituent C atom and N atom in the cyano groups, but antibonding interaction between carbon in the ring and carbon atom in the $-CN$ group, due to the back-donation from nitrogen to carbon. The abundant daughter ion percent of $C_6N_5^-$ can be explained by the most stable isomer obtained from the DFT calculation, but the ion fragment of $C_8N_5^-$ cannot be reasonably interpreted from this isomer, which indicates that besides the C_{2v} structure, the other isomers with higher energy can coexist in the cluster process.

5.1.5. $C_{18}N_7^-$. In the mass spectrum, $C_{18}N_7^-$ is presented as a very weak signal after the relatively intense mass peak of $C_{16}N_7^-$, which suggests that the instability of $C_{18}N_7^-$ compared with that of $C_{16}N_7^-$. When the carbon number exceeds 16 with the nitrogen number unchangeable, the increasing carbon atoms can only be added on the substituent group by extending the $-CN$ group. The differences for total energies of the isomers with the $-C_3N$ group linked to the different carbon atoms in the double-ring are small. From the NBO charge distribution in the relatively lowest energy isomer, we can see that extending the $-CN$ group to the $-C_3N$ group will bring little change for charge distribution on other atoms compared with that of $C_{16}N_7^-$.

In our experiment conditions by vacuum expansion, the products formed are mostly in their lowest energy structures, while a few may coexist as other higher energy isomers. The following are some characteristics in the lowest energy structures for these $C_{2n}N_7^-$ clusters in this work: (1) Except for $C_{16}N_7^-$, the isomer is closer to the structure of adenine the higher the stability, not the higher the symmetry the higher the stability. (2) With the increasing number of C atoms in these molecules, the N atoms in the backbone ring are gradually substituted by C atoms from the six-membered ring to the five-membered ring. And each time, the N atom with the relatively less negative charge in the ring of the lowest energy structure of $C_{2n}N_7^-$ is

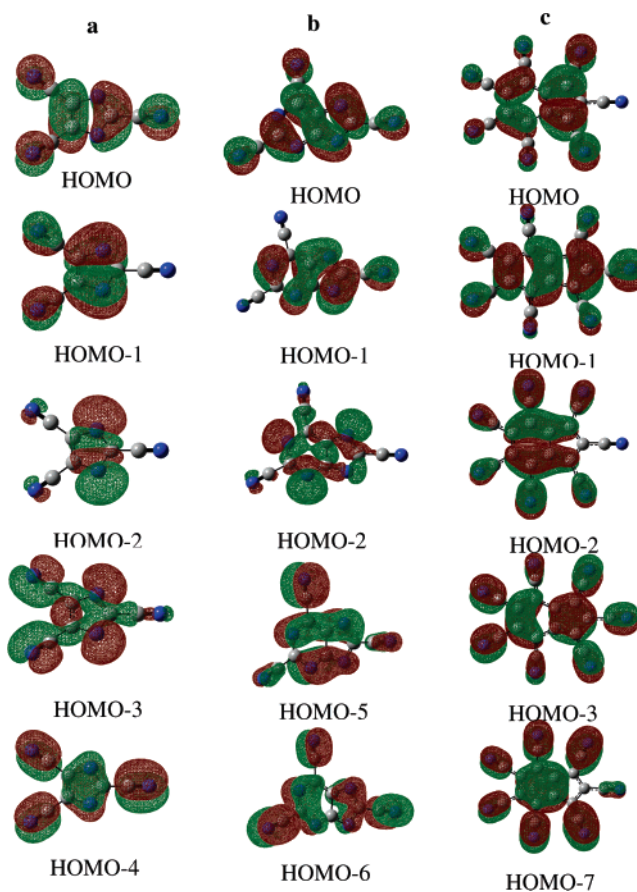


Figure 9. Molecular orbital pictures for (a) $C_6N_5^-$, (b) $C_8N_7^-$, and (c) $C_{16}N_7^-$.

substituted by a C atom and a $-CN$ group forming the stable $C_{2(n+1)}N_7^-$ structure. This also applies for the structure transformation from $C_6N_7^-$ to $C_8N_7^-$. This substitution of $-CN$ groups at different sites can be attributed to different charge distributions creating different stabilities for the different atoms. The substitution happens on the N atom with less negative charge in the ring because of its relatively lower stability. (3) The negative charge is distributed on the double-ring (all between -0.88 and $-0.92|e|$) rather than on the cyano groups. (4) The bond lengths in the cyano groups $C\equiv N$ in these

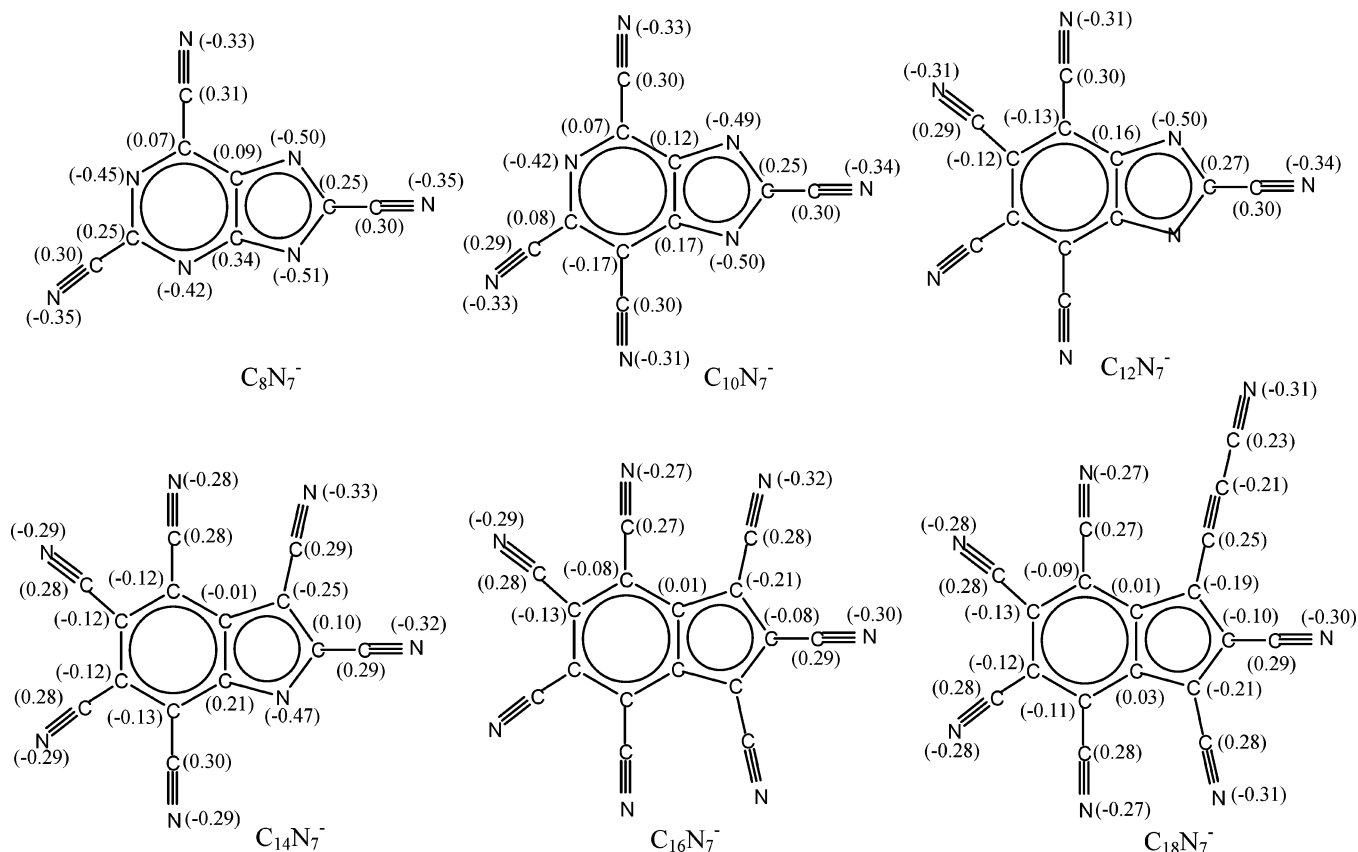


Figure 10. NBO charge distributions (in parentheses) of the most stable $C_{2n}N_7^-$ ($n = 4-9$) structures at the B3LYP/6-311+G(d) level.

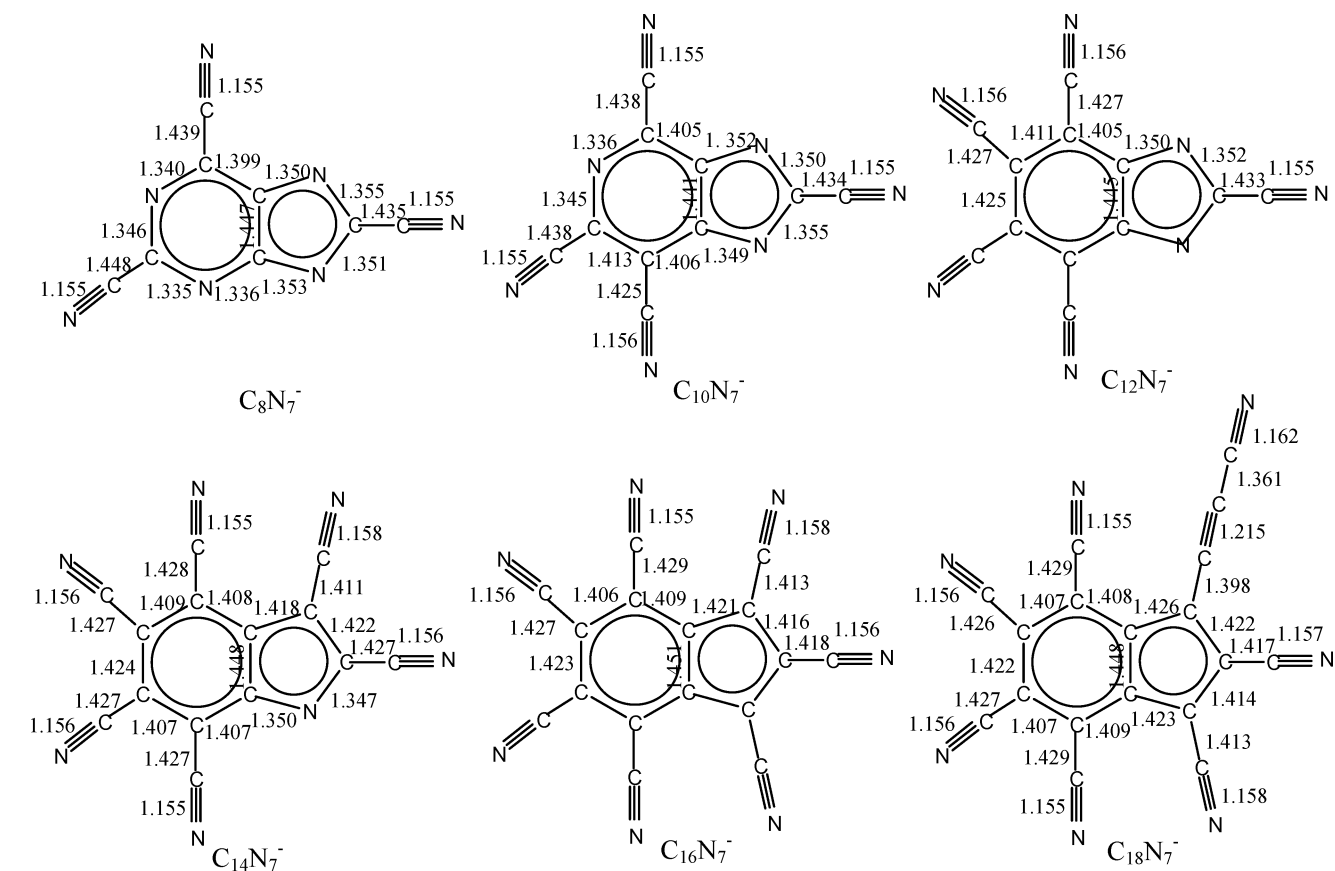


Figure 11. Bond lengths (in Å) of the most stable $C_{2n}N_7^-$ ($n = 4-9$) structures obtained at the B3LYP/6-311+G(d) level.

compounds are between 1.155 and 1.158 Å, in good agreement with the accepted value of 1.153 Å for HCN.⁴⁴ (5) All the C–C bond lengths including C–C in the backbone ring

and C–CN that connect cyano groups with the molecular ring are in the scope of 1.40–1.45 Å, near the bond length of the C–C value in benzene of 1.40 Å. (6) And C–N bonds in the

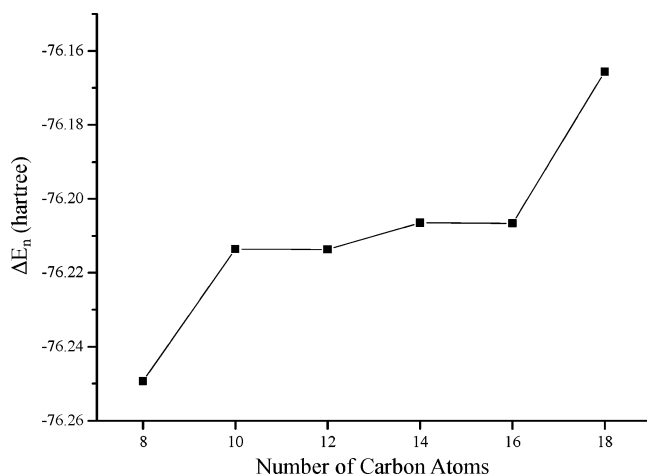


Figure 12. Energy differences ΔE_n (hartree) for the most stable $C_{2n}N_7^-$ ($n = 3-9$) structures vs the number of carbon atoms (as shown in Table 3).

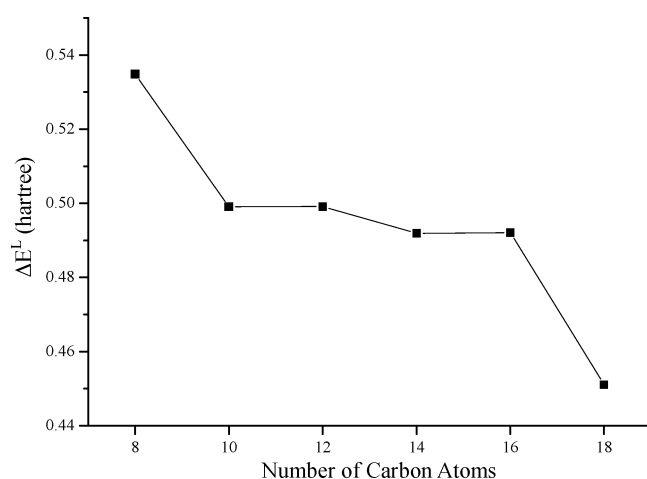


Figure 13. Incremental binding energies ΔE^L (hartree) for the most stable $C_{2n}N_7^-$ ($n = 3-9$) structures vs the number of carbon atoms (as shown in Table 3).

TABLE 3: Energy Difference (ΔE_n , in hartree), Atomization Energy (ΔE_a , in hartree), and Incremental Binding Energy (ΔE^L , in hartree) of the Lowest Energy Structures for $C_{2n}N_7^-$ ($n = 3-9$) Species at the B3LYP/6-311+G(d) Level

	ΔE_n	ΔE_a	ΔE^L
$C_6N_7^-$		2.667156	
$C_8N_7^-$	-76.249350	3.201972	0.534816
$C_{10}N_7^-$	-76.213557	3.700995	0.499023
$C_{12}N_7^-$	-76.213663	4.200124	0.499129
$C_{14}N_7^-$	-76.206464	4.692054	0.491930
$C_{16}N_7^-$	-76.206599	5.184119	0.492065
$C_{18}N_7^-$	-76.165590	5.635175	0.451056

skeleton double-ring are all between 1.33 and 1.36 Å, which are shorter than the C–N single bond length of 1.47 Å, but longer than the C=N double bond length of 1.28 Å. Therefore, according to the bond length analysis, we can see that the bond lengths in all these species are highly average and the π bonds are delocalized. Furthermore, the triple bond in the $-C\equiv N$ groups can be conjugated with the delocalized π bond of the ring so as to improve the stability of these species. The relatively high intensity of $C_8N_7^-$ and $C_{16}N_7^-$ in the mass spectrum may result from the adenine-like structure of $C_8N_7^-$ and the high geometric symmetry of $C_{16}N_7^-$.

5.2. Energy Difference and Incremental Binding Energy.

Table 3 lists the energy difference, atomization energy, and incremental binding energy for the lowest energy structures of

$C_{2n}N_7^-$ ($n = 3-9$) species. The energy difference ΔE_n is defined as $\Delta E_n = E(C_{2n}N_7^-) - E(C_{2(n-1)}N_7^-)$, which is calculated as the difference between the total energies (including correction for zero-point vibrational energies) of the adjacent clusters. The energy differences are close to each other from $C_8N_7^-$ to $C_{16}N_7^-$, which indicates that their stabilities are consecutive and no preferential stability and alternation appears. But the total energy from $C_6N_7^-$ to $C_8N_7^-$ decreases more than others, which suggests that $C_6N_7^-$ is unstable compared with $C_{2n}N_7^-$ ($n = 4-8$). And the absolute value for this energy difference between $C_{16}N_7^-$ and $C_{18}N_7^-$ is evidently smaller than the others, which indicates that $C_{18}N_7^-$ is also unstable compared with $C_{2n}N_7^-$ ($n = 4-8$). Moreover, the relative stability of the clusters can also be reflected by the incremental binding energy (ΔE^L),^{38,45-50} which is the energy difference between the atomization energies (ΔE_a : $\Delta E_a = 2nE(C) + 7E(N) - E(C_{2n}N_7^-)$) of the adjacent clusters. We have calculated the incremental binding energy (ΔE^L : $\Delta E^L = \Delta E_a(C_{2n}N_7^-) - \Delta E_a(C_{2(n-1)}N_7^-)$). Like the above energy differences, the incremental binding energies for clusters from $C_8N_7^-$ to $C_{16}N_7^-$ are also similar (about 0.5 hartree) to each other. But the incremental binding energy from $C_6N_7^-$ to $C_8N_7^-$ is obvious larger, while from $C_{16}N_7^-$ to $C_{18}N_7^-$ it is obvious smaller, which also suggests that the stability from $C_6N_7^-$ to $C_8N_7^-$ increases and that from $C_{16}N_7^-$ to $C_{18}N_7^-$ decreases. Such results are consistent with the experimental observation.

In the mass spectrum, the peaks for $C_nN_7^-$ ($n = 8-18$) with the odd-number carbon atoms are not observed, from which we can predict that the structures for the odd-number carbon atoms $C_nN_7^-$ clusters are distinctly different from those of the carbon–nitrogen clusters containing even-number carbon atoms and seven nitrogen atoms discussed in this paper, and $C_{2n}N_7^-$ clusters with even-number carbon atoms are more stable.

6. Conclusions

Interestingly, by laser ablating on the $K_3[Fe(CN)_6]$ sample, we have observed stable $C_{2n}N_7^-$ ($n = 4-9$) clusters in experiment. Different isomeric structures for these cluster anions have been optimized at the B3LYP/6-311+G(d) level and the lowest energy structures are found. More interestingly, by the structure analysis with theoretical calculation and CID experimental results, we find that the most stable structure for $C_8N_7^-$ is similar to that of adenine, with only the substituent groups changed. With the increasing number of C atoms in the $C_{2n}N_7^-$ series, the N atoms in the skeleton ring are gradually substituted by the C atoms and $-CN$ groups. And all the molecules exhibit aromatic characteristics. The stable $C_{2n}N_7^-$ ($n = 4-8$) clusters compared with relatively unstable $C_6N_7^-$ and $C_{18}N_7^-$ are explained according to the energy differences and incremental binding energies. This work shows progress for carbon–nitrogen cluster research.

Acknowledgment. We gratefully acknowledge the support of the National Natural Science Foundation of China under Grants 20203020 and 20433080.

Supporting Information Available: Figure 1S and Table 1S report optimized isomers for $C_6N_5^-$ and their parameters, Figure 2S gives bond lengths and NBO charge distributions for the most stable $C_6N_7^-$ isomer, Table 2S lists the energies for $C_{2n}N_7^-$ ($n = 3-9$) isomers by different basis sets, and Figure 3S shows MO pictures for $C_6N_7^-$, $C_{10}N_7^-$, $C_{12}N_7^-$, $C_{14}N_7^-$, and $C_{18}N_7^-$. This material is available free of charge via the Internet at <http://pubs.acs.org>.

References and Notes

- (1) Jefferts, K. B.; Penzias, A. A.; Wilson, R. W. *Astrophys. J. Lett.* **1970**, *161*, L87.
- (2) Turner, B. E. *Astrophys. J. Lett.* **1971**, *163*, L35.
- (3) Avery, L. W.; Brotten, N. W.; MacLeod, J. M.; Oka, T.; Kroto, H. W. *Astrophys. J. Lett.* **1976**, *205*, L173.
- (4) Guélin, M.; Thaddeus, P. *Astrophys. J. Lett.* **1977**, *212*, L81.
- (5) Brotten, N. W.; Oka, T.; Avery, L. W.; MacLeod, J. M.; Kroto, H. *Astrophys. J. Lett.* **1978**, *223*, L105.
- (6) Bell, M. B.; Feldman, P. A.; Kwok, S.; Matthews, H. E. *Nature* **1982**, *295*, 389.
- (7) Tang, Z. C.; Huang, R. B.; Shi, L.; Zheng, L. S. *Int. J. Mass. Spectrom. Ion Processes* **1998**, *173*, 71.
- (8) Ying, Z. C.; Hettich, R. L.; Compton, R. N.; Haufler, R. E. *J. Phys. B: At., Mol. Opt. Phys.* **1996**, *29*, 4935.
- (9) Clipston, N. L.; Brown, T.; Vasilev, Y. Y.; Barrow, M. P.; Herzschuh, R.; Reuther, U.; Hirsch, A.; Drewello, T. *J. Phys. Chem. A* **2000**, *104*, 9171.
- (10) Yu, R. Q.; Zhan, M. X.; Cheng, D. D.; Yang, S. Y.; Liu, Z. Y.; Zheng, L. S. *J. Phys. Chem.* **1995**, *99*, 1818.
- (11) Pradeep, T.; Vijayakrishnan, V.; Santra, A. K.; Rao, C. N. R. *J. Phys. Chem.* **1991**, *95*, 10564.
- (12) Glenis, S.; Cooke, S.; Chen, X.; Labes, M. M. *Chem. Mater.* **1994**, *6*, 1850.
- (13) Grosser, T.; Hirsch, A. *Angew. Chem., Int. Ed.* **1993**, *32*, 1340.
- (14) Jia, Y. F.; Zhu, Q.; Thomas, K. M. *Chem. Phys. Lett.* **2002**, *364*, 171.
- (15) Hummelen, J. C.; Knight, B.; Pavlovich, J.; Gonzalez, R.; Wudl, F. *Science* **1995**, *269*, 1554.
- (16) Nuber, B.; Hirsch, A. *Chem. Commun.* **1996**, *12*, 1421.
- (17) Lamparth, I.; Nuber, B.; Schick, G.; Skieba, A.; Grösser, T.; Hirsch, A. *Angew. Chem., Int. Ed.* **1995**, *34*, 2257.
- (18) Kim, K. C.; Hauke, F.; Hirsch, A.; Boyd, P. D. W.; Carter, E.; Armstrong, R. S.; Lay, P. A.; Reed, C. A. *J. Am. Chem. Soc.* **2003**, *125*, 4024.
- (19) Christian, J. F.; Wan, Z. M.; Anderson, S. L. *J. Phys. Chem.* **1992**, *96*, 10597.
- (20) Manaa, M. R.; Sprehn, D. W.; Ichord, H. A. *J. Am. Chem. Soc.* **2002**, *124*, 13990.
- (21) Hultman, L.; Stafström, S.; Czigány, Z.; Neidhardt, J.; Hellgren, N.; Brunell, I. F.; Suenaga, K.; Colliex, C. *Phys. Rev. Lett.* **2001**, *87*, 225503.
- (22) Liu, A. Y.; Cohen, M. L. *Science* **1989**, *245*, 841.
- (23) Niu, C. M.; Lu, Y. Z.; Lieber, C. M. *Science* **1993**, *261*, 334.
- (24) Teter, D. M.; Hemley, R. J. *Science* **1996**, *271*, 53.
- (25) BelBruno, J. J. *Chem. Phys. Lett.* **1997**, *270*, 99.
- (26) Jiang, J. C.; Cheng, W. J.; Zhang, Y.; Zhu, H. S.; Shen, D. Z. *Mater. Sci. Forum* **2005**, *480*, 71.
- (27) Yin, L. W.; Bando, Y.; Li, M. S.; Liu, Y. X.; Qi, Y. X. *Adv. Mater.* **2003**, *15*, 1840.
- (28) Zhang, Z. H.; Leinenweber, K.; Bauer, M.; Garvie, L. A. J.; McMillan, P. F.; Wolf, G. H. *J. Am. Chem. Soc.* **2001**, *123*, 7788.
- (29) Kroll, P.; Hoffmann, R. *J. Am. Chem. Soc.* **1999**, *121*, 4696.
- (30) Chen, Y.; Guo, L. P.; Wang, E. G. *Mod. Phys. Lett. B* **1996**, *10*, 615.
- (31) Chuhev, K.; BelBruno, J. J. *J. Phys. Chem. A* **2003**, *107*, 11217.
- (32) Chuhev, K.; BelBruno, J. J. *J. Phys. Chem. A* **2002**, *106*, 4240.
- (33) BelBruno, J. J.; Tang, Z. C.; Smith, R.; Hobday, S. *Mol. Phys.* **2001**, *99*, 957.
- (34) Jiang, Z. Y.; Xu, X. H.; Wu, H. S.; Jin, Z. H. *Int. J. Mass. Spectrom.* **2003**, *230*, 33.
- (35) Pascoli, G.; Lavendy, H. *Chem. Phys. Lett.* **1999**, *312*, 333.
- (36) McCarthy, M. C.; Fuchs, G. W.; Kucera, J.; Winnewisser, G.; Thaddeus, P. *J. Chem. Phys.* **2003**, *118*, 3549.
- (37) Wang, C. R.; Huang, R. B.; Liu, Z. Y.; Zheng, L. S. *Chem. Phys. Lett.* **1995**, *237*, 463.
- (38) Chen, M. D.; Liu, J. W.; Dang, L.; Zhang, Q. E. *J. Chem. Phys.* **2004**, *121*, 11661.
- (39) Tang, Z. C.; BelBruno, J. J.; Huang, R. B.; Zheng, L. S. *J. Chem. Phys.* **2000**, *112*, 9276.
- (40) Frisch, M. J.; Trucks, G. W.; Schlegel, H. B.; Scuseria, G. E.; Robb, M. A.; Cheeseman, J. R.; Zakrzewski, V. G.; Montgomery, J. A.; Stratmann, R. E.; Burant, J. C.; Dapprich, S.; Millam, J. M.; Daniels, A. D.; Kudin, K. N.; Strain, M. C.; Farkas, O.; Tomasi, J.; Barone, V.; Cossi, M.; Cammi, R.; Mennucci, B.; Pomelli, C.; Adamo, C.; Clifford, S.; Ochterski, J.; Petersson, G. A.; Ayala, P. Y.; Cui, Q.; Morokuma, K.; Malick, D. K.; Rabuck, A. D.; Raghavachari, K.; Foresman, J. B.; Cioslowski, J.; Ortiz, J. V.; Baboul, A. G.; Stefanov, B. B.; Liu, G.; Liashenko, A.; Piskorz, P.; Komaromi, I.; Gomperts, R.; Martin, R. L.; Fox, D. J.; Keith, T.; Al-Laham, M. A.; Peng, C. Y.; Nanayakkara, A.; Challacombe, M.; Gill, P. M. W.; Johnson, B.; Chen, W.; Wong, M. W.; Andres, J. L.; Gonzalez, C.; Head-Gordon, M.; Replogle, E. S.; Pople, J. A. *Gaussian 98*; Gaussian, Inc.: Pittsburgh, PA, 1998.
- (41) Chen, H.; Huang, R. B.; Lu, X.; Tang, Z. C.; Xu, X.; Zheng, L. S. *J. Chem. Phys.* **2000**, *112*, 9310.
- (42) Chen, H.; Huang, R. B.; Xie, Z. X.; Chen, L. H.; Zheng, L. S. *J. Chem. Phys.* **2001**, *114*, 812.
- (43) Broomhead, J. M. *Acta Crystallogr.* **1948**, *1*, 324.
- (44) Hehre, W. J.; Stewart, R. F.; Pople, J. A. *J. Chem. Phys.* **1969**, *51*, 2657.
- (45) Pascoli, G.; Lavendy, H. *Int. J. Mass. Spectrom.* **1998**, *173*, 41.
- (46) Pascoli, G.; Lavendy, H. *Int. J. Mass. Spectrom.* **1998**, *181*, 11.
- (47) Pascoli, G.; Lavendy, H. *Int. J. Mass. Spectrom.* **1998**, *181*, 135.
- (48) Pascoli, G.; Lavendy, H. *J. Phys. Chem. A* **1999**, *103*, 3518.
- (49) Lavendy, H.; Pascoli, G. *Int. J. Mass. Spectrom.* **1999**, *189*, 125.
- (50) Li, G. L.; Xing, X. P.; Tang, Z. C. *J. Chem. Phys.* **2003**, *118*, 6884.